

Nonlinear Optical Properties of Pyrene Derivatives Based on a Donor–Acceptor Structure and Its Polyurethane Composites

Lijun Gao,* Biyu Li, Haoyue Yi, Jing Cui, Linpo Yang, Yinglin Song, Hao-Ran Yang, Liming Zhou,* and Shaoming Fang*



Cite This: *ACS Omega* 2022, 7, 27959–27968



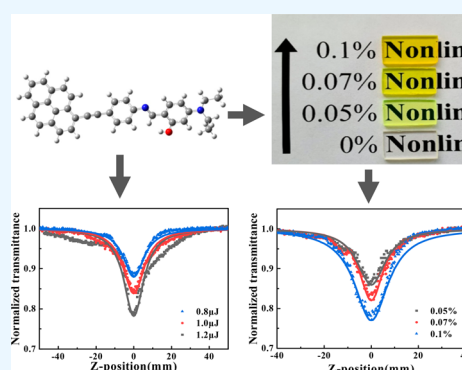
Read Online

ACCESS |

Metrics & More

Article Recommendations

ABSTRACT: Two pyrenyl Schiff base derivatives with π conjugated structures (**B2** and **B3**) were designed and synthesized. Then, **B2** and **B3** were added into polyurethane to obtain doped and bonded polyurethane nonlinear optical materials (**B2/PU** and **B3/PU**), respectively. The synthesized **B2**, **B3**, and polyurethane nonlinear optical materials were tested by a nanosecond (ns) and picosecond (ps) pulse Z-scan at a 532 nm wavelength. Due to the two-photon absorption-induced excited state absorption (TPA-ESA), **B2**, **B3**, and polyurethane nonlinear optical materials show reverse saturable absorption (RSA). From a quantum chemistry calculation, it can be concluded that the RSA of **B2** and **B3** comes from the large π conjugated system and intramolecular charge transfer. Furthermore, **B2**, **B3**, and the polyurethane nonlinear optical materials show good optical limiting. **B2/PU** and **B3/PU** not only have excellent nonlinear optical properties but also have good transmittance, thermal stability, and processability of polyurethane materials. The combination of pyrenyl Schiff base derivatives and polyurethane materials greatly improves the application of nonlinear small molecules in the field of optical limiting and all-optical switching.



1. INTRODUCTION

Nonlinear optics mainly concerns the study of nonlinear phenomena and applications of matter under the action of strong coherent light. In 1961, Franken¹ passed a pulse generated by a ruby laser through quartz crystal and observed the second harmonic for the first time. With the discovery of nonlinear optical phenomena such as stimulated Raman scattering, parametric oscillation, reverse saturation absorption, self-phase modulation, and so on, the research of nonlinear optics and related applications has developed at an unprecedented speed.^{2–6} In recent years, nonlinear optical materials have potential applications in optical information storage, all-optical switching, fluorescence microscopy, photodynamic therapy, etc.^{7–12} Nonlinear optical materials were first studied from inorganic materials, such as KTiOPO_4 (KTP) type materials, KH_2PO_4 (KDP) type materials, perovskite type materials, borate materials, and so on.^{13–15} Although inorganic materials as nonlinear optical materials have the advantages of good chemical stability, processing performance, and high frequency doubling conversion rate, the long-term development of inorganic materials is limited by the disadvantages of low damage threshold, low nonlinear response, and difficulty processing into devices. People's vision has gradually shifted from inorganic materials to organic materials. Organic nonlinear materials are popular because of their high nonlinear optical absorption coefficient, fast response, and easy

modification.^{13,16} For example, Schiff base compounds, azo compounds, and a series of other organic molecular materials with large π conjugated structures have low dielectric constants, easy modification and combination, and organic nonlinear materials with variable structures can be obtained by molecular design and synthesis.^{17–20} Schiff base materials are formed by the condensation of primary amine and carbonyl compounds, and the carbon nitrogen double bond can be used as a π electron bridge to construct a large π conjugated system, which greatly improves the mobility of intramolecular carriers and makes the whole system have a greater nonlinear optical response.^{19,21,22} In addition to organic small molecular materials, nonlinear polymer materials, such as polyacetylene (PA), polythiophene (PTH), polyaniline (PANI), and their derivatives, have become a research hotspot due to their high nonlinear optical coefficient, fast response time, excellent processing performance, and structural diversity.^{23–26}

In recent years, people have been looking for potential organic nonlinear materials with large π conjugated sys-

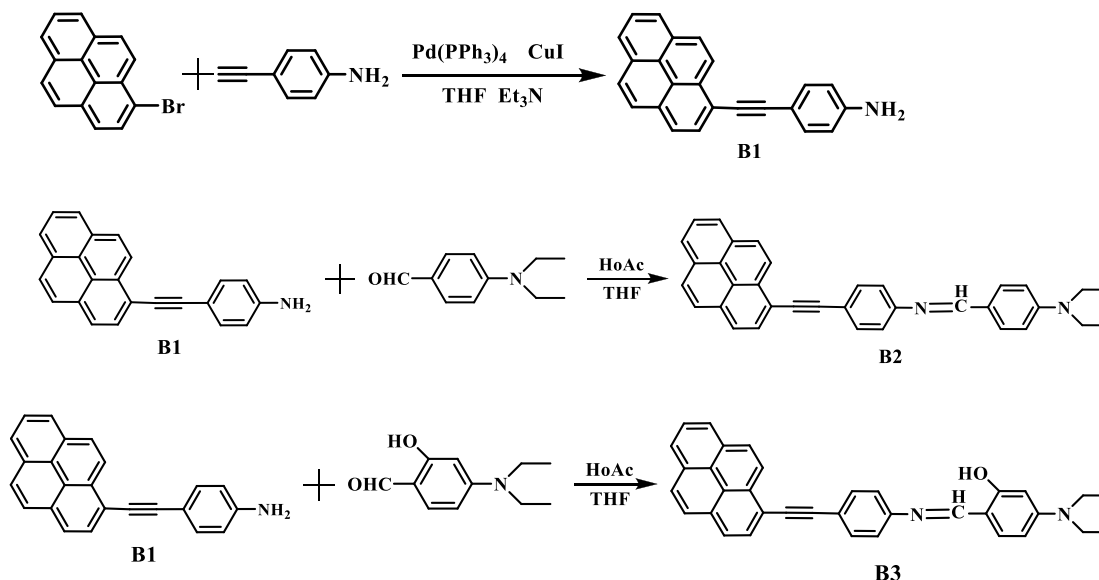
Received: March 23, 2022

Accepted: July 7, 2022

Published: August 3, 2022



Scheme 1. Synthesis Steps of Pyrenyl Schiff Base Derivatives



tems.^{27–29} Perylenetetracarboxylic diimide (PDI) and pyrene, as kinds of polycyclic aromatic hydrocarbons, not only have excellent fluorescence properties and electronic conductivity but also have large π conjugated rings and easy modification. They can be used as a structural unit to construct materials with excellent diversity and nonlinearity by controlling the number and types of substituents.^{30–33} In addition, alkyne bonds are widely used for the effective bonding of various groups to expand the π conjugated plane.^{34,35} The introduction of alkynes into polycyclic aromatic hydrocarbons (PAHs) can enlarge their π conjugated rings and greatly enhance the electron transport in the molecular system.^{36–40} In this context, two new pyrenyl Schiff base compounds with $D-\pi-A$ structures were synthesized with pyrene as the charge transfer acceptor and alkynyl and imine as the conjugated bridge to enhance the electron transport, to study the connection between the properties and structure of nonlinear small molecules. Furthermore, the two synthesized pyrenyl Schiff base derivatives were added into polyurethane (PU) to obtain polyurethane nonlinear optical materials, and the effect of the content of pyrenyl Schiff base derivatives on the properties of polyurethane nonlinear materials was studied in detail.

2. MATERIALS AND METHODS

2.1. Synthesis of Pyrenyl Schiff Base Compounds. B1, B2, and B3 compounds were prepared according to the route in Scheme 1.

Synthesis of B1. 1-Bromopyrene (2.24 g, 8 mmol), 4-ethynylaniline (0.94 g, 8 mmol), Pd(PPh₃)₄ (462 mg, 0.4 mmol), and CuI (76 mg, 0.4 mmol) were mixed in a flask, and then, dehydrated and deoxygenated solvents THF (35 mL) and Et₃N (35 mL) were added. The reaction was heated and stirred under nitrogen for 12 h. After the reaction, the solution was cooled to room temperature. After filtration, the solution was collected, and the crude product was obtained after drying. Further purification was performed by silica gel column chromatography with a mixture of petroleum ether and ethyl acetate as the eluent. An orange yellow solid (**B1**, 1.84 g, 72%) was obtained. ¹H NMR (400 MHz, chloroform-*d*) δ (ppm): 8.67 (d, *J* = 9.1 Hz, 1H), 8.28–7.97 (m, 8H), 7.54 (d, *J* = 8.3

Hz, 2H), 6.72 (d, *J* = 8.3 Hz, 2H), 3.88 (s, 2H). ¹³C NMR (150 MHz, chloroform-*d*) δ (ppm): 147.22, 132.43, 130.71, 130.64, 130.44, 130.02, 128.66, 127.55, 127.23, 126.70, 125.75, 125.03, 124.98, 124.89, 124.05, 123.82, 123.66, 118.11, 114.18, 110.96, 96.15, 85.7.

Synthesis of B2. **B1** (600 mg, 1.89 mmol) and 4-diethylaminobenzaldehyde (402 mg, 2.27 mmol) were mixed into a 100 mL flask, and then, dehydrated THF (35 mL) was added. A drop of acetic acid (HoAc) was added, and the reaction was heated and stirred for 12 h. After the reaction, the solution was cooled to 25 °C and dried with anhydrous Na₂SO₄. After the solvent was removed, further purification was performed by silica gel column chromatography with a mixture of petroleum ether and ethyl acetate (8:1) as the eluent. A yellowish brown solid (**B2**, 0.66 g, 73%) was obtained. ¹H NMR (400 MHz, chloroform-*d*) δ (ppm): 8.70 (d, *J* = 9.1 Hz, 1H), 8.36 (s, 1H), 8.26–8.00 (m, 8H), 7.78 (d, *J* = 8.6 Hz, 2H), 7.76–7.69 (m, 2H), 7.24 (s, 2H), 6.72 (d, *J* = 8.6 Hz, 2H), 3.45 (q, *J* = 7.0 Hz, 4H), 1.23 (t, *J* = 7.1 Hz, 6H). ¹³C NMR (150 MHz, chloroform-*d*) δ (ppm): 159.38, 151.63, 148.08, 132.38, 132.09, 130.95, 130.56, 130.41, 129.92, 128.97, 128.63, 127.89, 127.63, 127.25, 126.75, 125.92, 125.22, 124.92, 124.13, 123.71, 123.51, 120.63, 118.18, 117.20, 113.89, 110.56, 109.99, 44.02, 12.05.

Synthesis of B3. The preparation process of **B3** is similar to that of **B2**. **B1** (600 mg, 1.89 mmol) and 4-(diethylamino)salicylaldehyde (437 mg, 2.27 mmol) were mixed in dehydrated THF (35 mL). Finally, a yellowish brown solid **B3** (0.7 g, 75%) was obtained. ¹H NMR (400 MHz, chloroform-*d*) δ (ppm): 8.69 (d, *J* = 9.1 Hz, 1H), 8.48 (s, 1H), 8.28–7.98 (m, 8H), 7.73 (d, *J* = 8.3 Hz, 2H), 7.31 (d, *J* = 8.3 Hz, 2H), 7.19 (d, *J* = 8.8 Hz, 1H), 6.28 (dd, *J* = 8.7, 2.4 Hz, 1H), 6.22 (s, 1H), 3.43 (q, *J* = 7.1 Hz, 4H), 1.23 (t, *J* = 7.1 Hz, 6H). ¹³C NMR (150 MHz, chloroform-*d*) δ (ppm): 163.68, 159.57, 151.83, 147.37, 133.89, 132.22, 131.06, 130.58, 130.55, 130.38, 128.97, 127.86, 127.64, 126.69, 125.84, 125.14, 124.83, 124.07, 123.77, 123.58, 120.30, 119.71, 117.14, 108.21, 103.79, 96.87, 94.73, 88.51, 44.12, 12.15.

2.2. Preparation of Dopant B2/PU Materials. **B2** (39 mg, 0.08 mmol) and azodiisobutyronitrile (0.115 g, 0.7 mmol)

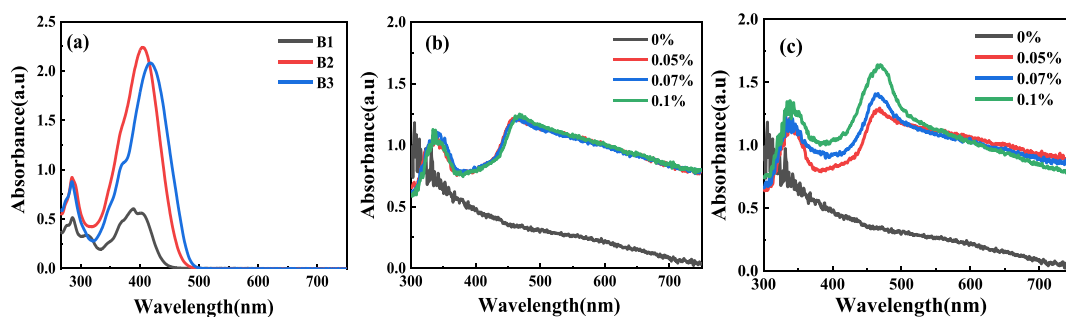


Figure 1. UV-vis absorption spectra of (a) B1, B2, and B3 in DMF; (b) B2/PU; and (c) B3/PU.

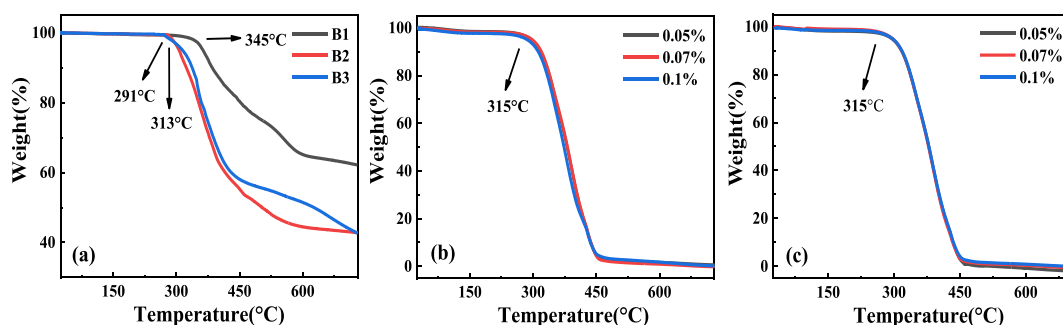


Figure 2. TG curves of materials: (a) B1, B2, and B3; (b) B2/PU; and (c) B3/PU.

were added to hydroxyethyl methacrylate (7.8 g, 0.06 mol) and mixed for 15 min until completely dissolved to obtain a mixed solution. Polyethylene glycol 600 (18 g, 0.03 mol) and isophorone diisocyanate (13.32 g, 0.06 mol) were stirred in a flask at 23 °C for 10 min, and the catalyst dibutyltin dilaurate (DBTL) (37 μ L) was also added and stirred for 20 min; then, the above mixed solution was added, and the mixture was stirred for 20 min. After stirring, the air in the mixture was pumped out by a vacuum pump, and the obtained prepolymer was poured into a self-made glass mold. The temperature was kept at 30, 40, 50, and 60 °C, separately, for 1 h, and then at 70 °C for 24 h. Finally, a B2/PU sheet with a thickness of 3 mm (B2 = 0.1 wt %) was obtained. By changing the content of B2 in the polyurethane sheet, B2/PU composites with B2 mass fractions of 0.05% and 0.07% were prepared, separately.

2.3. Preparation of Bonded B3/PU Materials. The preparation of bonded B3/PU materials is like that of doped polyurethane composites. B3 (39 mg, 0.079 mmol), polyethylene glycol 600 (18 g, 0.03 mol), and isophorone diisocyanate (13.32 g, 0.06 mol) were first mixed. Then, dibutyltin dilaurate (DBTL) (37 μ L), the mixed solution of hydroxyethyl methacrylate (7.8 g, 0.06 mol), and azodiisobutyronitrile (0.115 g, 0.7 mmol) were added and stirred. The plate making method is like that of B2/PU. B3/PU with B3 mass fractions of 0.05%, 0.07%, and 0.1% were prepared by changing the content of B3 in the polyurethane sheet.

2.4. Characterization and Methods. ^1H NMR and ^{13}C NMR spectra were collected on a 600 MHz Bruker Avance III NMR spectrometer. UV-vis absorption spectra were measured on a Hitachi U-3900H spectrophotometer. The transmittance was measured by a WGT-S instrument. The thermal stability was performed using an integrated thermal analyzer (Diamond TG/DTA). The nonlinear optical properties of the compounds were also tested by a Z-scan experiment with

different laser pulse widths. 15 ps pulses of 532 nm were obtained from a Q-switched Nd:YAG laser (1064 nm, 15 ps, 10 Hz). 4 ns pulses of 532 nm were obtained from a Q-switched Nd:YAG laser (1064 nm, 4 ns, 10 Hz). The laser source used for optical limiting experiments was the same as that used for the Z-scan. The compounds were dissolved in DMF with a concentration of 1 mg/mL. A 2 mm thick quartz dish was used as the test vessel.

3. RESULTS AND DISCUSSION

3.1. UV-Vis and Thermogravimetric Analysis. The UV-vis absorption spectra of B1, B2, and B3 are shown in Figure 1a. Figure 1 shows that the strong absorption bands of B2 and B3 are located at 285 and 405 nm, and 285 and 418 nm, respectively, attributed to the $\pi-\pi^*$ and $n-\pi^*$ electron transitions in the molecule. The absorption peak of B3 is red-shifted by 13 nm compared to that of B2. The energy needed for electron transition is decreased as the wavelength moves to the long wavelength. Because of the decrease of the HOMO-LUMO energy gap, the maximum absorption peak of B3 has a large red shift.^{41,42} Figure 1b,c shows the UV-vis absorption spectra of B2/PU and B3/PU. The absorption peaks of B2/PU and B3/PU composites are at 338 and 466 nm, and 338 and 463 nm, respectively. The intensity of the absorption band of polyurethane doped with different concentrations of B2 is basically the same, and the intensity is consistent with that of polyurethane doped with a minimum concentration of B3. This is because B2 is doped into the polyurethane sheet by simple physical blending, and a small change in the B2 doping amount will not cause a change in the light transmittance. However, the absorption band strength of the B3/PU composite increases with an increase in the B3 content because the hydroxyl group on B3 reacts with the active group

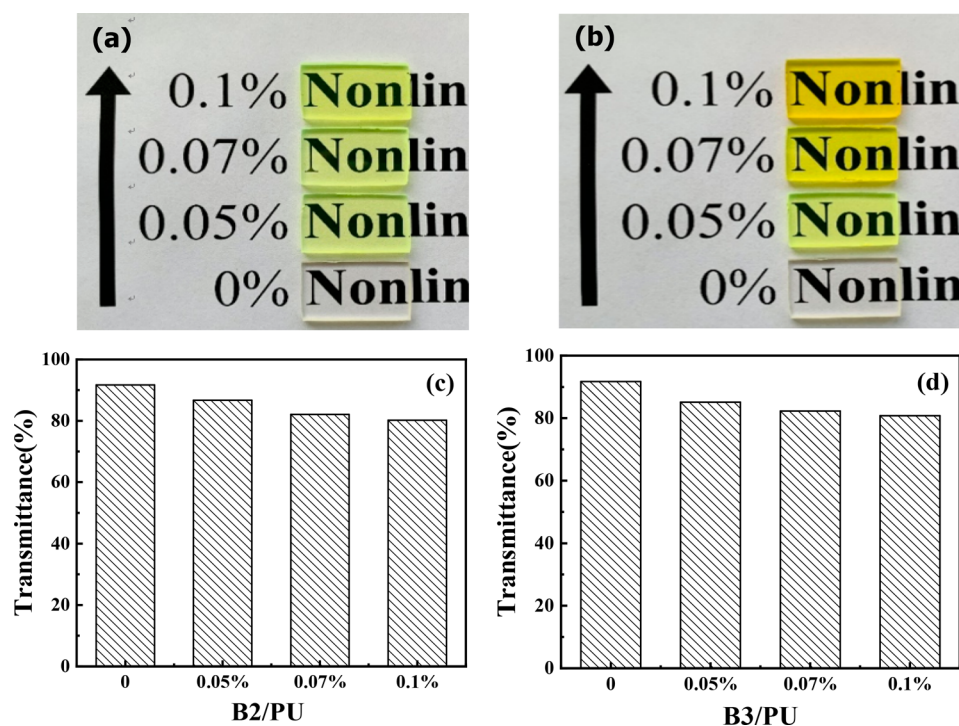


Figure 3. Pictures and transmittances of (a, c) B2/PU and (b, d) B3/PU composite materials with different contents of B2 or B3.

on diisocyanate, and finally, B3 is introduced into polyurethane by bonding.

The thermal stabilities of B1, B2, B3, B2/PU, and B3/PU were studied by thermogravimetric analysis at a heating rate of 10 °C/min in a N₂ atmosphere. It can be seen from Figure 2 that the epitaxial initial thermal decomposition temperatures of B1, B2, and B3 are 345, 313, and 291 °C, respectively. The thermal stability of the B2 compound is slightly higher than that of B3. The epitaxial initial thermal decomposition temperature of B2/PU and B3/PU is about 315 °C, and the thermal decomposition temperature of a polyurethane plate doped with a small amount of small molecules is basically the same, which shows that the thermal stability of both doped and bonded polyurethane composites depends on the thermal stability of the pure polyurethane plate; thus, improving the thermal decomposition temperature of the matrix plate is the key for its use as optical devices. In short, polyurethane composites have good thermal stability and processability and are expected to become optical device materials, which greatly expands the application of B2 and B3 in the optical field.

3.2. Transmittance of Polyurethane Composites. An image of the polyurethane composite is shown in Figure 3. The pure polyurethane plate is colorless and transparent, and the doped polyurethane plate is light yellow; with increases in the doping concentration, the color becomes darker. However, the doped plates have good optical transmittance and can be used as optical materials. The pure polyurethane material has the highest transmittance of 91.7%. The transmittances of B2/PU doped with 0.05%, 0.07%, and 0.1% are 86.7%, 82.1%, and 80.2%, respectively. The transmittances of B3/PU bonded with 0.05%, 0.07%, and 0.1% are 85.1%, 82.3%, and 80.8%, respectively.

It can be seen from the comparison of the data in the figure that the transmittance of the doped polyurethane plate and bonded polyurethane plate gradually decreases with increases in the mixing concentration, which is due to the red shift of the

UV absorption of the polyurethane composite toward the long-wave direction because of the addition of B2 and B3. B2/PU and B3/PU composites have high light transmittance, which will have good prospects in the field of optical devices.

3.3. Quantum Chemistry Calculation. For the sake of investigating the connection between the structures of B2 and B3 compounds and their nonlinear properties, the quantum chemistry of B2 and B3 has been calculated by density functional theory (DFT) at the B3LYP/6-31G(d) theoretical level in the Gaussian 09 program.^{43,44} Frontier molecular orbitals (HOMO orbitals and LUMO orbitals) of the two compounds are shown in Figure 4. Table 1 shows the

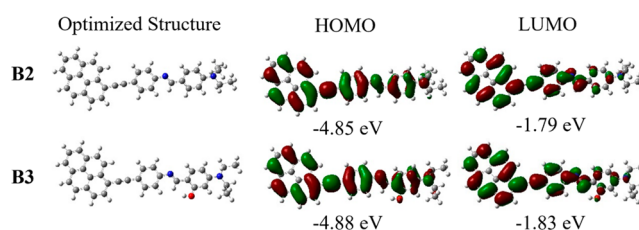


Figure 4. Frontier molecular orbital distribution of B2 and B3 extracted from DFT calculations.

occupancy of each component in the frontier molecular orbital. In Figure 4, the B2 and B3 compounds can be approximated as D- π -A structures, consisting of receptors, donors, and π conjugated bridges (alkynes, imines, and benzene rings). The possession proportion of the pyrene group in B2 changed from 57% to 88%, the possession proportion of the long conjugated bridge (alkyne, imine, and benzene ring) from 29% to 11%, and the possession proportion of the diethylamino group from 14% to 1%. The possession proportion of the pyrene group in B3 changed from 59% to 85%, the possession proportion of the long conjugated bridge (alkyne, imine and benzene ring)

Table 1. Possession Percentage That Each Component Occupied in the Frontier Molecular Orbitals of B2 and B3

		pyrene (%)	acetylene (%)	benzene (%)	imine (%)	<i>N,N</i> -diethylamine (terminal group %)
B2	HOMO	57	10	13	6	14
	LUMO	88	6	4	1	1
B3	HOMO	59	9	13	5	14
	LUMO	85	6	5	2	2

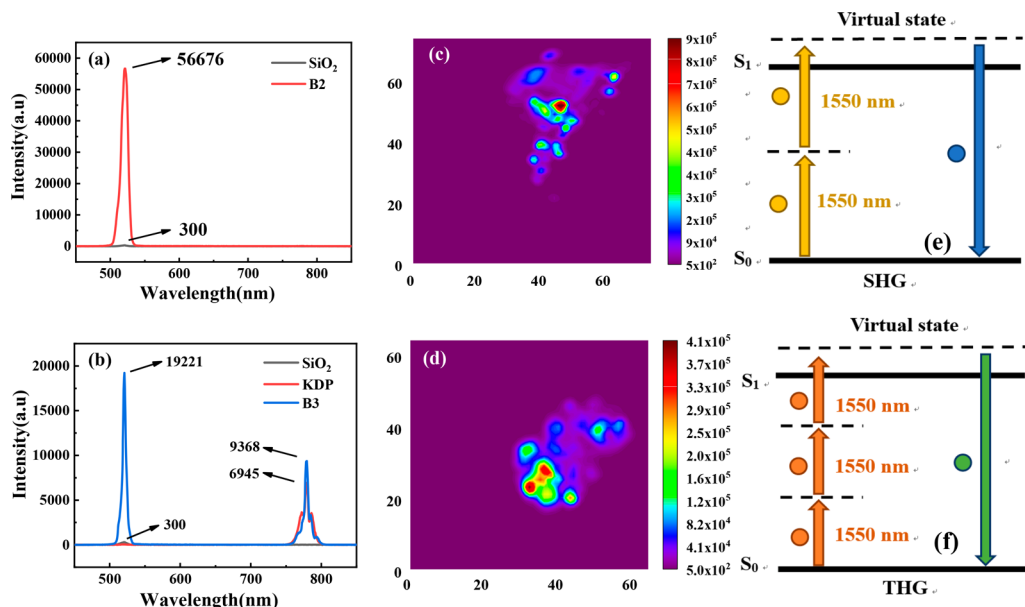


Figure 5. (a, b) Nonlinear spectra of SiO₂, KDP, B2, and B3 at a 1550 nm excitation wavelength. SHG and THG intensity mapping of (c) B2 and (d) B3 with the 1550 nm laser light source. Schematic diagram of the (e) SHG and (f) THG generation process.

from 27% to 13%, and the possession proportion of the diethylamino group from 14% to 2%. It is obvious that the electrons of B2 and B3 are transferred from the diethylamino group to the pyrene group through the conjugated bridge, demonstrating intramolecular charge transfer (ICT), and the charge transfer in B2 is slightly greater than that in B3.

Finally, it is concluded that ICT and the π conjugation system together affect the HOMO–LUMO transition of the two compounds. As can be seen from Table 1, the proportion of pyrene groups in the B2 system increases from 57% to 88%, and that in the B3 system increases from 59% to 85%, indicating that diethylamino acts as an electron donor and the pyrene group as an electron acceptor when HOMO transitions to LUMO. In Figure 4, the HOMO–LUMO energy gaps of B2 and B3 are 3.06 and 3.05 eV, respectively. Compared with B2, B3 has a smaller HOMO–LUMO energy gap. This is because, in B2 and B3 compounds, charge transfer plays a leading role, and the pyrene groups of the two molecules have obvious π – π^* transitions. The hydroxyl group on the B3 molecule is connected with the benzene ring, and part of the π – π^* transition is converted to the n – π^* transition; the transition energy is reduced. The presence of a benzene ring and conjugate bridge increases the π conjugate plane and reduces the energy of electron transition. The results of the quantum chemistry calculation are consistent with the UV–vis absorption spectra.

3.4. NLO Properties of B2 and B3. Second harmonic generation (SHG) and third harmonic generation (THG) are two kinds of nonlinear optical phenomena. The anisotropy of the material may result in high second-order nonlinear polarizability ($\chi^{(2)}$), third-order nonlinear polarizability ($\chi^{(3)}$),

and harmonic signals.^{45,46} In Figure 5, two fundamental incident photons are converted into a new frequency-doubling photon in the nonlinear material, which is the generation process of the second harmonic. The third harmonic generation process is similar. Three fundamental incident photons are converted into a new frequency multiplier photon in the nonlinear material, which is the generation process of the third harmonic. The second and third harmonics are generated without energy conversion, which will not affect the test compounds.

The nonlinear optical signals of B2 and B3 were tested by a 1550 nm laser, with potassium dihydrogen phosphate (KDP) and silicon dioxide (SiO₂) as standard samples to collect signals of 300–900 nm.^{16,47,48} In Figure 5, B2 has a sharp peak at 517 nm, corresponding to one-third of the incident light at 1550 nm, presenting THG characteristics. B3 has sharp peaks at 517 and 775 nm and has the characteristics of SHG and THG. Compared with B2, B3 shows THG and SHG signals at the same time, because B3 has the hydroxyl group in its structure, which destroys the central symmetry of the system.⁴⁷ The overall signal intensity is weaker than B2, which may be because B3 has SHG and THG at the same time, and the SHG signal affects the THG signal intensity of B3. B3 has the characteristics of SHG and THG, while B2 only has the characteristics of THG. It can be inferred that B3 is more inclined to noncentrosymmetric crystals than B2.^{47,49} Under the same test conditions, the THG intensities of B2 and B3 are, respectively, 188 times and 64 times that of SiO₂, and the SHG intensity of B3 is 1.3 times that of KDP. Therefore, both B2 and B3 compounds have good SHG and THG properties.

The SHG and THG properties of the two compounds can be used in optical communication and signal processing fields.

A schematic diagram of the Z-scan test is shown in Figure 6. The Z-scan is performed by translating the sample along the Z

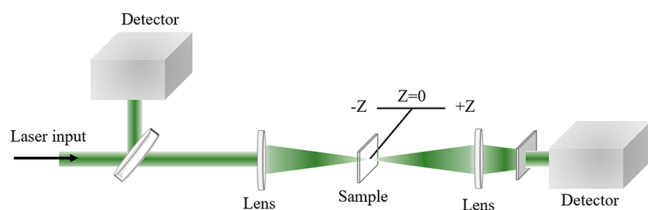


Figure 6. Schematic diagram of the Z-scan test.

axis from one side of the focus to the other. The light spot area of the incident sample changes with the change of the sample Z position. When the incident pulse energy is constant, the change in the light spot area is equivalent to the change in the incident light intensity. By detecting the energy change through the sample under different light intensities, the absorption strength of the sample under different light intensities can be obtained. The nonlinear absorption of B2 and B3 compounds was studied by Z-scan. The same Z-scan test was performed for pure DMF, but no absorption signal was observed, ruling out the effect of DMF on compound absorption. The two compound solutions with the concentration of 1 mg/mL were placed in a 2 mm thick quartz dish for the Z-scan test. In Figure 7, the Z-scan curves of B2 and B3

compound solutions show antisaturation; furthermore, the points are the experimental data, and the real lines are the theoretical fitting result. The absorption of B2 and B3 compounds is enhanced near the focal point, indicating positive nonlinear absorption, also known as antisaturation absorption (RSA).⁵⁰ The antisaturation absorption of the compound also increased when the test laser was intensified. Under the same test conditions, the absorption of B2 and B3 compounds is roughly the same, but the B3 compound has a wider broadband RSA, which is more suitable for the field of light limiting.

The nonlinear absorption coefficient (β) was obtained by fitting the experimental results.⁵¹ In Table 2, β increases with

Table 2. Nonlinear Absorption Coefficients (β) of B2 and B3 Extracted in Z-Scan Experiments

E (μJ)	ns		ps		
	β (10^{-11} m/W)		β (10^{-11} m/W)		
	B2	B3	E (μJ)	B2	B3
10.2	3.3	4.1	0.8	0.37	0.73
20.2	4.5	4.9	1.0	0.43	0.84
30.3	4.8	5.8	1.2	0.70	0.92

increasing laser energy, which is the excited state absorption induced by two-photon absorption (TPA-ESA).^{52,53} At the same energy, the β value of B3 is higher than that of B2, because B3 has a hydroxyl group in its structure. In B2 and B3,

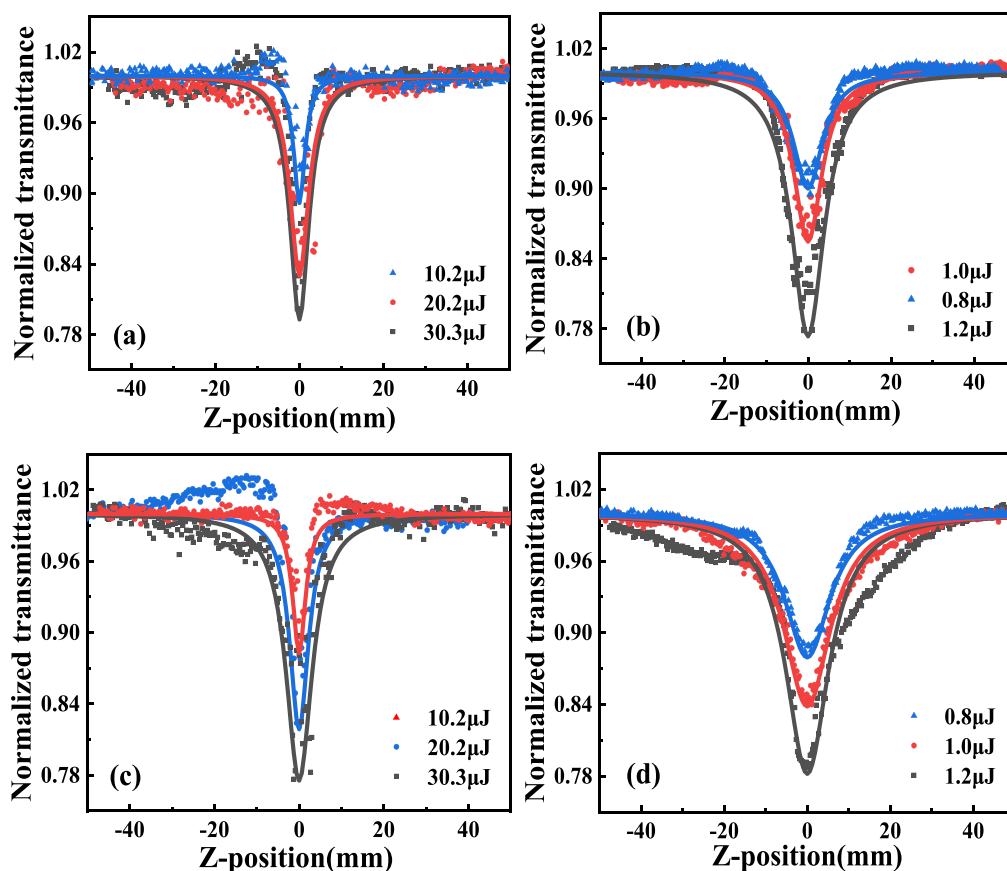


Figure 7. Z-scan curves of (a, b) B2 for ns and ps and (c, d) B3 for ns and ps. The points are the test result, and the real curve is the theoretical fitting results.

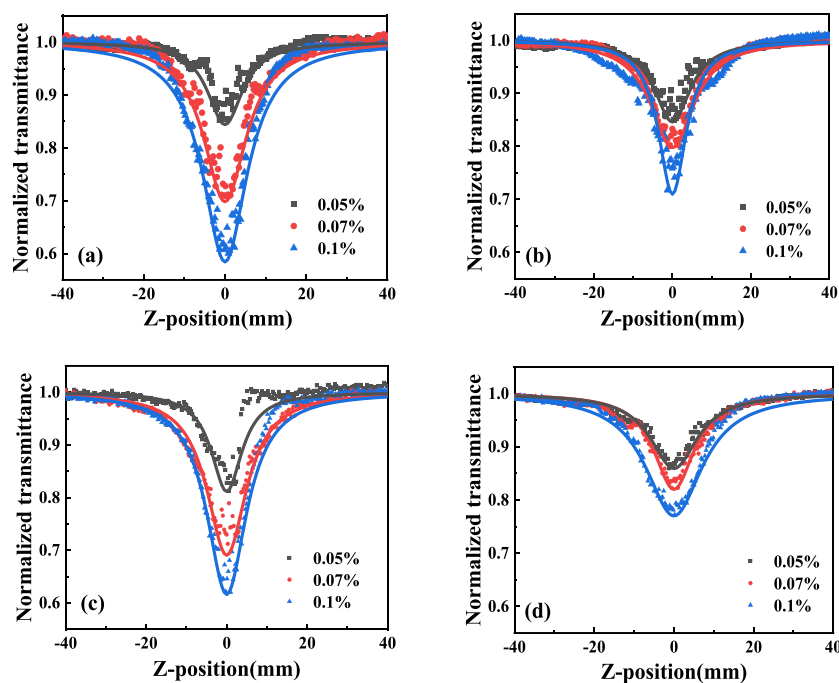


Figure 8. Z-scan curves of (a, b) B2/PU for ns and ps and (c, d) B3/PU for ns and ps. The points are the test result, and the solid curves are the theoretical fitting results.

charge transfer plays a leading role in transition, but pyrene groups of both molecules have a $\pi-\pi^*$ transition. When the benzene ring on compound B3 is connected to the hydroxyl group, the intramolecular electron transfer mode partially changes from $\pi-\pi^*$ transition to $n-\pi^*$ transition, and the energy required for the electron transition decreases, which makes the molecule have stronger RSA. Although electron transfer and π conjugation enhance the nonlinear absorption of molecules, electron transfer plays a decisive role in the nonlinear absorption of materials. In addition, B2 and B3 have a greater RSA coefficient than similar pyrene derivatives.³⁰ This is because the carbon–nitrogen double bond and alkyne bond as the conjugate bridge not only improve the conjugation length of the molecule but also keep the π conjugated surface of pyrene and other groups as much as possible in the same plane and greatly increase intramolecular charge transfer, effectively improving RSA. Finally, B2 and B3 have good nonlinear absorption and broadband RSA, which can be used as potential optical limiting materials. The hydroxyl active group in B3 greatly expands the application range.

3.5. NLO Properties of Polyurethane Composites. The nonlinear optical absorption of B2/PU and B3/PU was studied by an Nd:YAG laser (532 nm, 15 ps, 10 Hz) and Nd:YAG laser (532 nm, 4 ns, 10 Hz). The ps laser energy is 1 μ J and the ns laser energy 20 μ J. In Figure 8, B2/PU and B3/PU show a good RSA capability under ns and ps conditions, and the RSA strength gradually increases with the increase of B2 and B3 content, indicating that the RSA capability of the polyurethane composite mainly comes from B2 and B3. Therefore, it is of practical significance to adjust the nonlinear optical properties of the composites by changing the amount of B2 and B3 in polyurethane materials. For the sake of comparing the nonlinear optical properties of polyurethane composites with different concentrations of B2 and B3, the experimental results were fitted, and the β values of

polyurethane composites were obtained. It can be seen from Figure 8 and Table 3 that the nonlinear absorption of

Table 3. Nonlinear Absorption Coefficients (β) of B2/PU and B3/PU Extracted in Z-Scan Experiments

mass fraction (%)	ns		ps		
	β (10^{-11} m/W)		β (10^{-11} m/W)		
	B2/PU	B3/PU	mass fraction (%)	B2/PU	B3/PU
0.05	8	13	0.05	0.75	0.74
0.07	22	20	0.07	0.92	0.80
0.1	38	26	0.1	1.00	0.88

polyurethane composites gradually increases with the increase of B2 and B3 amount, and β increases proportionally. When the amount of added B2 and B3 is 0.05%, the β fitted by B3/PU under the ns and ps laser is greater than that of B2/PU. Also, with a gradual increase in the amount added, when it is 0.07% and 0.1%, the β of B2/PU and B3/PU improves greatly, but the β of B3/PU is also greater than that of B2/PU. The nonlinear performances of B2/PU and B3/PU is better than those of B2 and B3. The improvement of optical nonlinear properties of B2/PU and B3/PU may be due to the cross-linked grid in the polyurethane matrix providing better dispersion space for B2 and B3, which makes them difficult to agglomerate or aggregate and makes the properties of materials more stable. Thus, the polyurethane composites with nonlinear small molecules not only retain the nonlinear optical properties of small molecules but also have good thermal stability and processing properties of polyurethane, which effectively promotes its application in optoelectronic and optical limiting fields.

The optical limiting performances of B2, B3, B2/PU, and B3/PU are studied using a 532 nm laser source. Figure 9 shows the optical limiting curve. The optical limiting threshold (F_{th}) is defined as the incident energy flow when the nonlinear

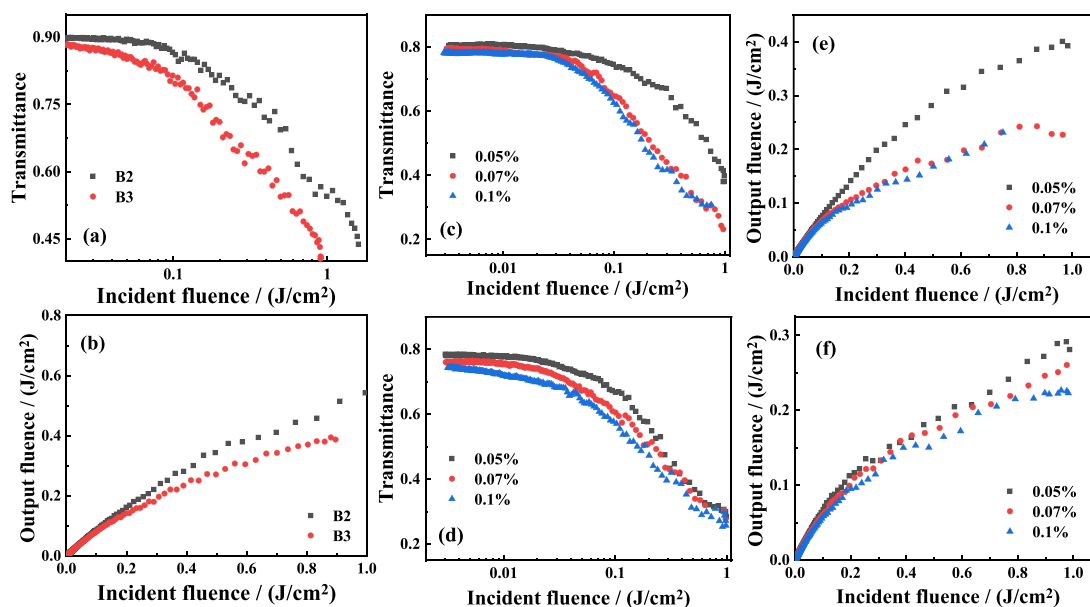


Figure 9. Picosecond optical limiting of (a, b) B2 and B3, (c, e) B2/PU, and (d, f) B3/PU under 532 nm.

transmittance of the material is reduced to half of the original value.⁵⁴ In Figure 9, when the laser energy increases, the transmittances of B2, B3, B2/PU, and B3/PU decrease by varying degrees, indicating that B2, B3, and polyurethane composites have a certain optical limiting ability. The optical limiting thresholds of B2 and B3 are 1.57 and 0.87 J/cm², respectively. Compared with B2, B3 has a lower optical limiting threshold, which indicates that its optical limiting ability is better. The optical limiting thresholds of B2/PU and B3/PU are 0.97 and 0.46 J/cm², respectively, when the amount added is 0.05%. The optical limiting thresholds of B2/PU and B3/PU decrease with increases in B2 and B3. When the content of B2 and B3 is 0.1%, the optical limiting thresholds of B2/PU and B3/PU are 0.35 and 0.4 J/cm², respectively. The optical limiting threshold decreases, and the optical limiting ability increases. The smaller optical limiting threshold is attributed to the stronger RSA, which is consistent with the Z-scan results. Compared with that of B2/PU, the reduction range of the optical limiting threshold of B3/PU is very uniform; because B3 is bonded with polyurethane, B3 is more evenly dispersed in polyurethane, and polyurethane with a small amount of B3 has a good optical limiting performance. The overall results show that B2, B3, B2/PU, and B3/PU all have good optical limiting abilities. The polyurethane composites not only have the original properties of polyurethane but also have better optical limiting properties.

4. CONCLUSION

B2 and B3 show good nonlinear optical properties and a good optical limiting ability under different pulse widths (ns and ps). The composites composed of B2, B3, and polyurethane not only retain the original properties of polyurethane but also have small molecular nonlinear optical properties. In general, B2/PU and B3/PU have good nonlinear properties; B3 is more evenly dispersed in polyurethane by bonding, and the nonlinear properties are more stable. It is more suitable to be used as an optical limiting material. Small molecules with nonlinear optical properties are introduced into polyurethane, which makes possible small molecules with nonlinear proper-

ties from experiment to applications. This series of polyurethane composites will have a good prospect in the application of nonlinear optical devices.

AUTHOR INFORMATION

Corresponding Authors

Lijun Gao – Henan Provincial Key Laboratory of Surface & Interface Science, College of Material and Chemical Engineering, Zhengzhou University of Light Industry, Zhengzhou 450000, China; orcid.org/0000-0002-0123-3805; Email: gljsuzanne@163.com

Liming Zhou – Henan Provincial Key Laboratory of Surface & Interface Science, College of Material and Chemical Engineering, Zhengzhou University of Light Industry, Zhengzhou 450000, China; Email: zlm1212@126.com

Shaoming Fang – Henan Provincial Key Laboratory of Surface & Interface Science, College of Material and Chemical Engineering, Zhengzhou University of Light Industry, Zhengzhou 450000, China; Email: fangshaoming@zzuli.edu.cn

Authors

Biyou Li – Henan Provincial Key Laboratory of Surface & Interface Science, College of Material and Chemical Engineering, Zhengzhou University of Light Industry, Zhengzhou 450000, China

Haoyue Yi – Henan Provincial Key Laboratory of Surface & Interface Science, College of Material and Chemical Engineering, Zhengzhou University of Light Industry, Zhengzhou 450000, China

Jing Cui – Henan Provincial Key Laboratory of Surface & Interface Science, College of Material and Chemical Engineering, Zhengzhou University of Light Industry, Zhengzhou 450000, China

Linpo Yang – Department of Physics, Harbin Institute of Technology, Harbin 150001, China

Yinglin Song – Department of Physics, Harbin Institute of Technology, Harbin 150001, China

Hao-Ran Yang – Henan Provincial Key Laboratory of Surface & Interface Science, College of Material and Chemical Engineering, Zhengzhou University of Light Industry, Zhengzhou 450000, China

Complete contact information is available at:
<https://pubs.acs.org/10.1021/acsomega.2c01751>

Notes

The authors declare no competing financial interest.

ACKNOWLEDGMENTS

The authors are sincerely thankful for the support of National Natural Science Foundation of China (U1704256, 21671178, and 21571159), the Basic and Frontier Technology Research Program of Henan Province (162300410033), and Zhongyuan Science and Technology Innovation Leading Talents (214200510017).

REFERENCES

- (1) Franken, P. A.; Hill, A. E.; Peters, C. W.; Weinreich, G. Generation of optical harmonics. *Phys. Rev. Lett.* **1961**, *7*, 118–119.
- (2) Gibbs, H. M.; McCall, S. L.; Venkatesan, T. Differential gain and bistability using a sodium-filled fabry-perot interferometer. *Phys. Rev. Lett.* **1976**, *36*, 1135–1138.
- (3) Eckhardt, G.; Hellwarth, R. W.; McClung, F. J.; Schwarz, S. E.; Woodbury, E. J. Stimulated raman scattering from organic liquids. *Phys. Rev. Lett.* **1962**, *9*, 455–457.
- (4) Giordmaine, J. A.; Miller, R. C. Optical parametric oscillation in the visible spectrum. *Phys. Rev. Lett.* **1966**, *9*, 298.
- (5) Garmire, E.; Chiao, R. Y.; Townes, C. H. Dynamics and characteristics of the self-trapping of intense light beams. *Phys. Rev. Lett.* **1966**, *16*, 347–349.
- (6) Ishiwata, T.; Tanaka, I. Stepwise two-photon excitation of Cl₂ to the E(0_g⁺) ion-pair state. *Phys. Rev. Lett.* **1984**, *107*, 434–437.
- (7) Xu, L.; Zhang, J. Z.; Yin, L. F. Recent progress in efficient organic two-photon dyes for fluorescence imaging and photodynamic therapy. *J. Mater. Chem. C* **2020**, *8*, 6342–6349.
- (8) Wang, R. F.; Cheng, Z. Y.; Deng, X. C. Photo-crosslinkable second order nonlinear AB₂-type monomers: convenient synthesis and enhanced NLO thermostability. *J. Mater. Chem. C* **2020**, *8*, 6380–6387.
- (9) Shan, Y. X.; Wu, L. M.; Liao, Y. L. A promising nonlinear optical material and its applications for all-optical switching and information converters based on the spatial self-phase modulation (SSPM) effect of TaSe₂ nanosheets. *J. Mater. Chem. C* **2019**, *7*, 3811–3816.
- (10) Raju, G. S. R.; Pavitra, E.; Lee, H. Pre-ouzo effect derived fergusonite gadolinium ortho-niobate mesoporous nanospheroids for multimodal bioimaging and photodynamic therapy. *Appl. Surf. Sci.* **2020**, *505*, 144584.
- (11) Pourtabrizi, M.; Shahtahmassebi, N.; Sharifmoghdam, M. R. Bromophenol blue doped in nano-droplet: spectroscopy, nonlinear optical properties and staphylococcus aureus treatment. *Opt Quantum Electron* **2021**, *53*, 1–13.
- (12) Jiang, D. Q.; Song, H. M.; Wen, T. Pressure-driven two-step second-harmonic-generation switching in BiOIO₃. *Angew. Chem., Int. Ed.* **2022**, *61*, 1–6.
- (13) Wu, J. Y.; Li, Z. A.; Luo, J. D. High-performance organic second- and third-order nonlinear optical materials for ultrafast information processing. *J. Mater. Chem. C* **2020**, *8*, 15009–15026.
- (14) Jiang, G. B.; Miao, L. L.; Yi, J.; Huang, B.; Peng, W.; Zou, Y. H.; Huang, H. H. Ultrafast pulse generation from erbium-doped fiber laser modulated by hybrid organic-inorganic halide perovskites. *Appl. Phys. Lett.* **2017**, *110*, 161111.
- (15) Wang, J.; Blau, W. J. Inorganic and hybrid nanostructures for optical limiting. *J. Opt. A* **2009**, *11*, 024001.
- (16) Yu, J. C.; Cui, Y. J.; Wu, C. D.; Yang, Y.; Wang, Z. Y. Second-order nonlinear optical activity induced by ordered dipolar chromophores confined in the pores of an anionic metal-organic framework. *Angew. Chem., Int. Ed.* **2012**, *51*, 10542–10545.
- (17) Hassan, Q. M. A.; Raheem, N. A.; Emshary, C. A. Preparation, DFT and optical nonlinear studies of a novel azo-(beta)-diketone dye. *Opt Laser Technol.* **2022**, *148*, 107705.
- (18) Lin, C. Pyridine vs N-hydrogenated pyridine moieties: theoretical study of stability and spectroscopy of nitrogen-contained heterocyclic aromatic compounds and graphene nanoflakes. *ACS Omega* **2018**, *3*, 12312–12319.
- (19) Derkowska-Zielinska, B.; Barwiolek, M.; Cassagne, C. Non-linear optical study of Schiff bases using Z-scan technique. *Opt Laser Technol.* **2020**, *124*, 105968.
- (20) Almashal, F. A.; Mohammed, M. Q.; Hassan, Q. M. A.; Emshary, C. A.; Sultan, H. A.; Dhumad, A. M. Spectroscopic and thermal nonlinearity study of a schiff base compound. *Opt. Mater.* **2020**, *100*, 109703.
- (21) Derkowska-Zielinska, B.; Barwiolek, M.; Cassagne, C.; Boudebs, G. Nonlinear optical study of schiff bases using z-scan technique. *Opt. Laser Technol.* **2020**, *124*, 105968.
- (22) Jassem, A. M.; Hassan, Q. M. A.; Almashal, F. A. Spectroscopic study, theoretical calculations, and optical nonlinear properties of amino acid (glycine)-4-nitro benzaldehyde-derived Schiff base. *Opt. Mater.* **2021**, *122*, 111750.
- (23) Waszkowska, K.; Chtouki, T.; Krupka, O. Effect of uv-irradiation and zno nanoparticles on nonlinear optical response of specific photochromic polymers. *Nanomater.* **2021**, *11*, 492.
- (24) Kulagina, A. S.; Sandulenko, A. V.; Volynkin, V. M. Synthesis and nonlinear optical properties of vanadium-doped plasticized epoxy polymer composites. *Advanced Composites and Hybrid Materials*, **2021**, *4*, 324–331.
- (25) Li, Z.; Zang, X.; Li, Y. Tetracyanobutadienyl-based nonlinear optical dendronized hyperbranched polymer synthesized via facile [2 + 2] cycloaddition polymer postfunctionalization. *Macromol. Rapid Commun.* **2022**, No. 2200179.
- (26) Zhao, F.; Pan, Z.; Wang, C.; Zhou, Y.; Qin, M. Third-order nonlinear optical properties of an azobenzene-containing ionic liquid crystalline polymer. *Opt. Quant. Electron.* **2014**, *46*, 1491–1498.
- (27) Long, X. T.; Wu, J. Y.; Yang, S. R. Discovery of and insights into one-photon and two-photon excited ACQ-to-AIE conversion via positional isomerization. *J. Mater. Chem. C* **2021**, *9*, 11679–11689.
- (28) Wang, T. F.; Huang, W. B.; Sun, T. Two-dimensional metal-polyphthalocyanine conjugated porous frameworks as promising optical limiting materials. *ACS Appl. Mater. Interfaces* **2020**, *12*, 46565–46570.
- (29) Jia, J. D.; Zhang, X. R.; Wang, Y. X. Enhanced two-photon absorption of cross-conjugated chalcone derivatives: modulation of the effective π -conjugated structure. *J. Phys. Chem. A* **2020**, *124*, 10808–10816.
- (30) Wang, X.; Wang, D.; Gao, H.; Yang, Z.; Cao, H.; Yang, H.; He, W.; Wang, H.; Gu, J.; Hu, H. Third-order nonlinear optical properties of a novel series of D- π -A pyrene-aldehyde derivatives. *J. Nonlinear Opt. Phys.* **2016**, *25*, 1650014.
- (31) Huang, G. B.; Shen, L.; Liu, J. Synthesis, self-assembly and nonlinear optical activity of selenium-annulated perylene diimide. *ChemComm* **2020**, *56*, 3123–3126.
- (32) Mariz, I. F. A.; Raja, S.; Silva, T. Two-photon absorption of perylene-3,4,9,10-tetracarboxylic acid diimides: Effect of substituents in the bay. *Dyes Pigm.* **2021**, *193*, 109470.
- (33) Sanusi, K.; Nyokong, T. Effects of pyrene on the photophysical and two-photon absorption-based nonlinear optical properties of indium(III) phthalocyanines. *J. Coord. Chem.* **2014**, *67*, 2911–2924.
- (34) Saal, A.; Friebe, C.; Schubert, U. S. Polymeric blatter's radical via CuAAC and ROMP[J]. *Macromol. Chem. Phys.* **2021**, *222*, 2100194.
- (35) Bao, M.; Xie, X. D.; Hu, W. H. Gold-catalyzed carbocyclization/C = N bond formation cascade of alkyne-tethered diazo compounds with benzo [c] isoxazoles for the assembly of 4-iminonaphthalenones and Indenes. *Adv. Synth. Catal.* **2021**, *363*, 4018–4023.

- (36) Platonova, Y. B.; Volov, A. N.; Tomilova, L. G. Palladium(II) phthalocyanines efficiently promote phosphine-free sonogashira cross-coupling reaction at room temperature. *J. Catal.* **2020**, *391*, 224–228.
- (37) Shaw, R.; Elagamy, A.; Althagafi, I.; Pratap, R. Synthesis of alkynes from non-alkyne sources. *Org. Biomol. Chem.* **2020**, *18*, 3797–3817.
- (38) Tang, S. X.; Wang, N.; Xu, X. D.; Feng, S. Y. A ratiometric fluorescent thermometer based on amphiphilic alkynylpyrene derivatives. *New J. Chem.* **2019**, *43*, 6461–6464.
- (39) Oh, J. W.; Kim, T. H.; Yoo, S. W.; Lee, Y. O.; Lee, Y. Multisignaling metal sensor: optical, electrochemical, and electrochemiluminescent responses of cruciform-shaped alkynylpyrene for selective recognition of Fe³⁺. *Sens. Actuators B Chem.* **2013**, *177*, 813–817.
- (40) Ramirez, M.; Darzi, E. R.; Donaldson, J. S. Cycloaddition cascades of strained alkynes and oxadiazinones. *Angew. Chem., Int. Ed.* **2021**, *60*, 18201–18208.
- (41) Srinivasan, V.; Panneerselvam, M.; Pavithra, N. A combined experimental and computational characterization of D- π -A dyes containing heterocyclic electron donors. *J. Photoch. Photobio. A* **2017**, *332*, 453–464.
- (42) Dubinina, T. V.; Osipova, M. M.; Zasedatelev, A. V. Synthesis, optical and electrochemical properties of novel phenyl- and phenoxy-substituted subphthalocyanines. *Dyes Pigm.* **2016**, *128*, 141–148.
- (43) Raj, M. R.; Anandan, S.; Solomon, R. V. Conjugated polymer based on oligobenzo[c]thiophene with low-lying homo energy level as potential donor for bulk heterojunction solar cells. *J. Photoch. Photobio. A* **2013**, *262*, 34–44.
- (44) Jagadeesan, R.; Velmurugan, G.; Venuvalingam, P. Rational design of cyclopenta[b]naphthalenes for better optoelectronic applications and their photophysical properties using DFT/TD-DFT methods. *RSC Adv.* **2016**, *6*, 44569–44577.
- (45) Zhou, X.; Cheng, J.; Zhou, Y.; Cao, T. Strong second-harmonic generation in atomic layered gase. *J. Am. Chem. Soc.* **2015**, *137*, 7994–7997.
- (46) Kulyk, B.; Waszkowska, K.; Busseau, A.; Villegas, C.; Sahraoui, B. Penta(zinc porphyrin)[60]fullerenes: strong reverse saturable absorption for optical limiting applications. *Appl. Surf. Sci.* **2020**, *533*, 147468.
- (47) Cammarata, A.; Zhang, W.; Halasyamani, P. S.; Rondinelli, J. M. Microscopic origins of optical second harmonic generation in noncentrosymmetric-nonpolar materials. *Chem. Mater.* **2014**, *26*, 5773–5781.
- (48) Liu, M.; Quah, H. S.; Wen, S.; Yu, Z.; Vittal, J. J.; Ji, W. Efficient third harmonic generation in a metal-organic framework. *Chem. Mater.* **2016**, *28*, 3385–3390.
- (49) Wu, C.; Yang, G.; Humphrey, M. G.; Zhang, C. Recent advances in ultraviolet and deep-ultraviolet second-order nonlinear optical crystals. *Coord. Chem. Rev.* **2018**, *375*, 459–488.
- (50) Kumar, T. R.; Vijay, R. J.; Jeyasekaran, R.; Selvakumar, S.; Arockiaraj, M. A.; Sagayaraj, P. Growth, linear and nonlinear optical and, laser damage threshold studies of organometallic crystal of MnHg(SCN)₄. *Opt. Mater.* **2011**, *33*, 1654–1660.
- (51) Sheik-Bahae, M.; Said, A. A.; Wei, T.; Hagan, D. J.; Stryland, E. W. V. Sensitive measurement of optical nonlinearities using a single beam. *IEEE J. Quantum Electron.* **1990**, *26*, 760–769.
- (52) Sutherland, R. L.; Brant, M. C.; Heinrichs, J.; Rogers, J. E. Excited-state characterization and effective three-photon absorption model of two-photon-induced excited-state absorption in organic push-pull charge-transfer chromophores. *J. Opt. Soc. Am. B* **2005**, *22*, 1939–1948.
- (53) Morel, Y.; Irimia, A.; Najechalski, P.; Kervella, Y.; Stephan, O. Two-photon absorption and optical power limiting of bifluorene molecule. *J. Chem. Phys.* **2001**, *114*, 5391–5396.
- (54) Liang, C. L.; Wang, E. Z.; Li, X. Optical limiting performances of transitional metal dichalcogenides MX₂ (M = V, Nb, Ta; X = S, Se) with ultralow initial threshold and optical limiting threshold. *Chin. Opt. Lett.* **2022**, *20*, 021901.